DINAME 2023 - Proceedings of the XIX International Symposium on Dynamic Problems of Mechanics,
A.S. De Paula, A.T. Fabro and M.R. Machado (Editors), ABCM.
Pirenópolis, Go, Brazil, February 26th to March 3rd, 2023

Dynamic Modes Decomposition of The Transonic Flow Around a Cylinder

Guilherme M. Santana[1], **Roberto F. B. Miserda**[1], **Adriano T. Fabro**[1]

[1] University of Brasilia, Faculty of Technology, Department of Mechanical Engineering, 70910900, Brasilia, Brazil

Abstract: This work aims at investigating the Dynamic Modes Decomposition as a tool to generate a Reduced-Order Model that captures adequately the noise generated by the transonic flow past a cylinder. This case was chosen because although it is relatively simple, it contains interesting dynamic features such as the wake and the acoustic field upwind of the cylinder. The extracted dynamic modes showed that the acoustic field can be decomposed as acoustic multipoles, and the decomposition of the wake revealed structures consistent with the literature. The reconstruction of the flow field with the projection of the pressure snapshots on the left singular vectors had a better agreement with the original time series, when compared to the reconstruction with DMD modes, but both methods were capable of properly capturing the frequency of the pressure fluctuations.

Keywords: Dynamic Modes Decomposition, Reduced-Order Model, Computational Aeroacoustics, Transonic Flow

INTRODUCTION

The majority of modern computational aeroacoustic studies are based on the Direct Noise Computation or on the use of linear equations to model noise propagation. Even though both methods can be adequately applied to several cases, the former usually has a high computational cost, while the later involves simplifying hypotheses that are often not satisfied in reality. An interesting alternative to these methods might be the use of a Reduced-Order Model (ROM) of the system of interest. A particularly interesting possibility as a method to obtain a ROM is the Dynamic Modes Decomposition (DMD). The DMD was originally presented by Schmid and Sesterhenn (2008) and Schmid (2010) as a method for the modal decomposition of a set of data that describes a dynamical system. The DMD uses a series of data snapshots of the system of interest to identify coherent structures, called dynamic modes, with associated frequencies and rates of growth or decay. An interesting aspect of the DMD method, as can be seen from the algorithm presented in the next section, is that it consists basically of the decomposition of a matrix that contains the data from a dynamic system, and does not involve, explicitly, a mathematical model of the dynamical system.

This independence from mathematical models allows the DMD to be directly used to analyze experimental results. Schmid (2010) applied the DMD to Particle Image Velocimetry (PIV) results for the flow past a flexible membrane and to the flow past an array of cylinders. Schmid *et al.* (2011) also used the DMD to extract the dynamic modes from Schlieren photographs of a helium jet. Ali *et al.* (2016) used the DMD to remove noise and identify the dominant structures inside an acoustic cavity exited with speakers. The authors applied the DMD to the pressure field, measured with fast-response pressure sensitive paint, over one of the cavity walls.

The DMD has also been extensively used to analyze the results from numerical simulations. Schmid (2010) used the DMD to calculate dynamic modes of the incompressible flow over a square cavity with a Reynolds number of 4500, and it was possible to identify stable and unstable modes. Sarmast *et al.* (2014) used numerical simulations to study instability of blade tip vortexes on the wake of a horizontal axis wind turbine. With the DMD, the authors were able to identify unstable modes associated with the interaction between vortexes of consecutive spirals and were able to formulate an analytical model to determine the length of the stable wake. Alenius *et al.* (2015) and Nair *et al.* (2016) applied the DMD to results from Large Eddy Simulations (LES) of the flow past an orifice plate, and were able to identify the coherent structures in the flow that generate noise. Nichols *et al.* (2017) used the DMD to study results from Large Eddy Simulations of the interaction of shock waves and boundary layers, and were able to identify a low frequency flow structure associated to the movement of the separation bubble and the shock wave, and a high frequency structure associated to the propagation of instability waves. The low frequency DMD mode was similar to some weakly stable oscillatory modes obtained with a Global Stability Analysis.

In addition to its applications in the identification of relevant characteristics of dynamical systems, the DMD has also been used, either by itself or in combination with other methods, as a method to obtain a reduced order model of complex systems. Tu and Rowley (2012) used a variation of the DMD algorithm to identify the modes that dominate the long term response of a system. With this, the authors were able to improve an algorithm for the balanced Proper Orthogonal Decomposition (POD) of a system, which resulted in a ROM with a much smaller computational cost an comparable accuracy, when compared to the standard balanced POD. Williams *et al.* (2013) used the DMD, combined with the POD method, to propose a hybrid, reduced order, numerical integrator capable of solving nonlinear PDEs with a fraction of the computational cost of the full simulation. The DMD is also included in the modred library for model decomposition

and reduced order model calculation (Belson *et al.*, 2014), and was used by Tissot *et al.* (2014) to provide a ROM for the wake of the flow past a cylinder, based on experimental data.

The objective of this work is to study the original DMD algorithm as a method to provide a ROM that properly describes the acoustic field generated by the transonic flow past a cylinder.

DYNAMIC MODES DECOMPOSITION

In this section, the Dynamic Modes Decomposition (DMD) is briefly presented. The DMD algorithm, as described by Kutz *et al.* (2016), consists initially of gathering a series of m snapshots of the flow of interest, sampled with an interval of Δt, that are organised into column vectors of two matrices $\mathbf{X}$ and $\mathbf{X}^{'}$, as

$$\mathbf{X} = \begin{bmatrix} | & | & & | \\ \mathbf{x}_1 & \mathbf{x}_2 & \cdots & \mathbf{x}_{m-1} \\ | & | & & | \end{bmatrix} \quad \text{and} \quad \mathbf{X}^{'} = \begin{bmatrix} | & | & & | \\ \mathbf{x}_2 & \mathbf{x}_3 & \cdots & \mathbf{x}_{m} \\ | & | & & | \end{bmatrix}. \tag{1}$$

It is then possible to write the equation for a discrete-time, equivalent linear system as

$$\mathbf{X}^{'} = \mathbf{A}\mathbf{X}. \tag{2}$$

where $\mathbf{A}$ is the matrix that represents the approximated discrete time, linear dynamics of the system. In order to minimise the error $\left\|\mathbf{X}^{'} - \mathbf{A}\mathbf{X}\right\|_F$, the linear operator $\mathbf{A}$ is given by $\mathbf{A} = \mathbf{X}^{'}\mathbf{X}^{\dagger}$, where $\dagger$ indicates the Moore-Penrose pseudo-inverse matrix of $\mathbf{X}$. It is possible to interpret these equations as a linear regression of the data onto the dynamics described by the linear operator $\mathbf{A}$. The eigenvectors of $\mathbf{A}$ are the dynamic modes, or DMD modes, and the corresponding eigenvalues indicate the frequency and rate of growth or decay of the mode.

However, the matrix $\mathbf{A}$ is of dimension $n \times n$, and the size of the snapshots, n, is generally large, which means it may not be possible to compute the eigendecomposition of $\mathbf{A}$ directly. A more efficient approach is to first calculate the singular value decomposition (SVD) approximation of $\mathbf{X}$ with a reduced order r, given by $\mathbf{X} \approx \mathbf{U}\Sigma\mathbf{V}^{*}$, where $\mathbf{U}$ and $\mathbf{V}$ are orthogonal matrices of dimensions $n \times r$ and $m \times r$, respectively, $*$ indicates the conjugate transpose and Σ is a diagonal matrix of dimensions $r \times r$. A reduced matrix with dimensions $r \times r$, the projection of $\mathbf{A}$ onto the left singular vectors (columns of matrix $\mathbf{U}$, also known as the Proper Orthogonal Decomposition (POD) modes), is given by

$$\tilde{\mathbf{A}} = \mathbf{U}^{*}\mathbf{A}\mathbf{U} = \mathbf{U}^{*}\mathbf{X}^{'}\mathbf{V}\Sigma^{-1}. \tag{3}$$

Since $\tilde{\mathbf{A}}$ is of much lower dimension than $\mathbf{A}$, its eigendecomposition can be efficiently calculated as $\tilde{\mathbf{A}}\mathbf{W} = \mathbf{W}\Lambda$, where the columns of $\mathbf{W}$ are the eigenvectors and Λ is a diagonal matrix with the eigenvalues. The eigenvectors of $\mathbf{A}$, which are the DMD modes ϕ_k can be recovered from $\mathbf{W}$ as the columns of the matrix Φ given by

$$\Phi = \mathbf{X}^{'}\mathbf{V}\Sigma^{-1}\mathbf{W}. \tag{4}$$

It is possible to use the DMD modes to make predictions of the dynamical system by writing the linear combination of the DMD modes weighted by their initial coefficients $\mathbf{b}$,

$$\mathbf{x}(t) = \Phi \exp(\Omega t)\,\mathbf{b}, \tag{5}$$

where Ω is a diagonal matrix with $\omega_k = \ln(\lambda_k)/\Delta t$, $\mathbf{b} = \Phi^{\dagger}\mathbf{x_1}$ and $\mathbf{x_1}$ is the initial snapshot.

Given the reduced-order matrix $\tilde{\mathbf{A}}$ and the left singular vectors $\mathbf{U}$ (Kutz *et al.*, 2016), it is also possible to write

$$\tilde{\mathbf{x}}_{k+1} = \tilde{\mathbf{A}}\tilde{\mathbf{x}}_k, \tag{6}$$

which is the reduced-order equation for the equivalent linear system given by Eq. (2). Starting from an initial condition $\tilde{\mathbf{x}}_0 = \mathbf{U}^{*}\mathbf{x}_0$, it is possible to reconstruct the full state $\mathbf{x}_k = \mathbf{U}\tilde{\mathbf{x}}_k$ at any instant $t = k\Delta t$ by a series of iterations of Eq. (6).

TRANSONIC FLOW PAST A CYLINDER

The flow around a cylinder is one of the most classical problems in fluid dynamics and the transonic case in particular has been studied in detail both experimentally and numerically, by Gowen and Perkins (1952), Rodriguez (1984) and Hughes and Tezduyar (1984), for example. This case was chosen because, even though it is a very simple bi-dimensional problem, it contains interesting dynamic features.

Computational Aspects

The data set used in this paper is the result of a numerical simulation of the transonic flow past a cylinder, modelled with Euler Equations for a compressible flow. The numerical method uses a finite volumes spatial discretization, a third order Runge-Kutta scheme for the time march and an immersed boundary method to apply the boundary conditions over the cylinder surface. This method is described with more detail by Miserda *et al.* (2020).

To reach the transonic regime and, at the same time, to prevent the flow from being too complex and difficult to study with the DMD method, the Mach number for the undisturbed flow was set to 0.5. The mesh size for the regular region of the domain is $D/128$, where D is the diameter of the cylinder, and the regular region has dimensions of $25D \times 25D$. This results in flow snapshots with $10,240,000$ grid points, and, with the computational resources available, it is possible to use 400 snapshots for the DMD calculation. To ensure the extremities of the domain are anechoic, there is a stretched region of the computational domain, were the size of the control volumes grows with a geometric progression with a ratio of 1.05.

Flow Results

Figure 1a shows one of the pressure snapshots used for the analysis. Figure 1b shows the flow field at the same instant as Fig. 1a, but with a visualisation variable called β_T and defined as $\beta_T = |\nabla T|^{1/10}$.

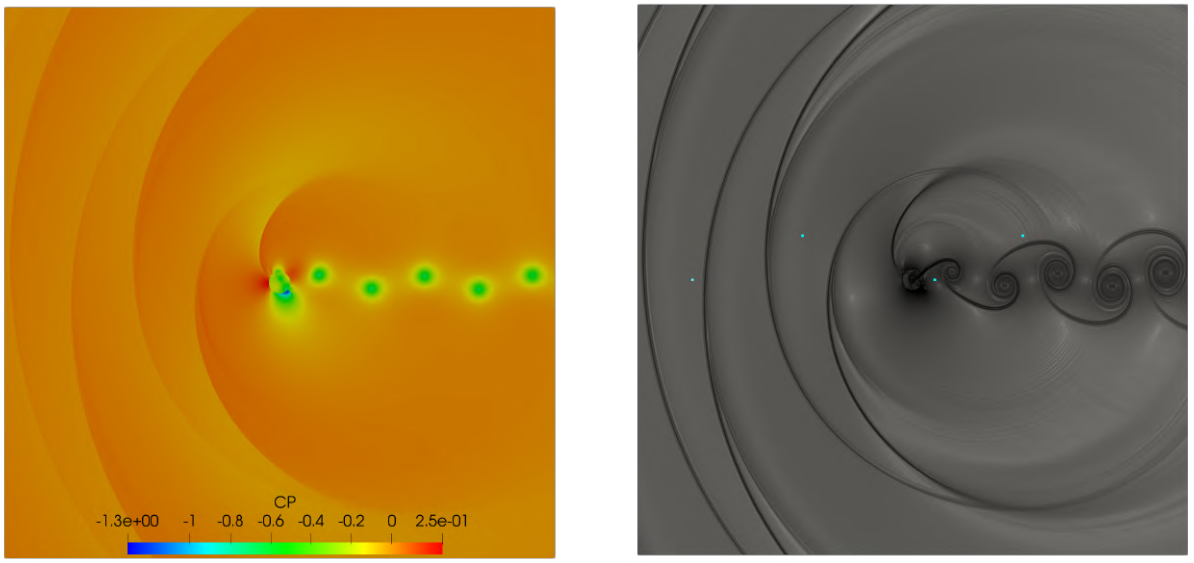

(a) Pressure field snapshot for the transonic flow past a cylinder.

(b) β_T field snapshot for the transonic flow past a cylinder.

Figure 1: Flow snapshots

The β_T variable was chosen because the temperature gradient in compressible flows is often more sensible to change than other properties, and the power of $1/10$ has the effect of bringing the aerodynamic and acoustic fluctuations to the same order of magnitude, which allows both phenomena to be observed in the same figure. Note how it is possible to see acoustic waves propagating downwind from the cylinder in Fig. 1b that just do not appear in Fig. 1a.

It is possible to observe that, even though the boundary layer is not modelled, there is flow separation due to the adverse pressure gradients associated with the shock waves formed at the top and at the bottom of the cylinder, which results in a periodic wake. Another interesting flow feature is the detachment and propagation of the shock waves, which results in an acoustic field upwind of the cylinder. This propagation of shock waves is compatible with the experimental results from Gowen and Perkins (1952), as well as the oscillating shock waves at the separation points.

Figure 2 shows the Sound Pressure Level field, defined as

$$SPL = 20\log_{10}\left(\frac{p'_{rms}}{2\times 10^{-5}}\right), \tag{7}$$

were p'_{rms} is the root mean square value of the pressure fluctuations $p' = p - \overline{p}$.

It is possible to observe from Fig. 2 that the shock waves formed at the top and the bottom of the cylinder result

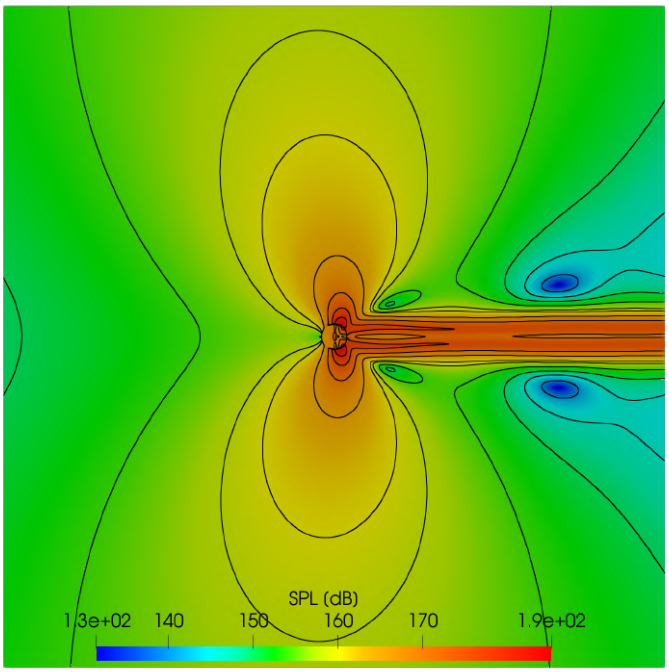

Figure 2: Sound Pressure Level field.

in an acoustic dipole, with the sound propagating preferentially in the direction orthogonal to the undisturbed flow. It also shows the pseudonoise at the wake, associated with the passage of the low-pressure vortex cores. This is called pseudonoise because the pressure fluctuations are not distinguished from the acoustic fluctuations in Eq. 7. But, unlike the acoustic ones, they propagate with the velocity of the flow instead of the sound velocity. In addition, there are two regions of silence, where the intensity of the sound is small when compared to the rest of the flow.

RESULTS

In this section, the DMD of the proposed case are investigated. Subsequently, they are used to reconstruct the pressure signal at some selected measurement probes and the results are compared to a projection on the left singular vectors with Eq. (6).

DMD Modes

The DMD method is applied to data snapshots of the pressure field for the transonic flow past a cylinder. Figure 3 shows some selected DMD modes, calculated with Eq. (4). The wake part of the modes is consistent with results from Kutz *et al.* (2016) for the DMD of the incompressible flow past a cylinder. There are some differences, but they can be explained by the use of pressure instead of vorticity snapshots and by the use of the Euler equations instead of the Navier-Stokes. It is also possible to observe from Fig. 3 that the acoustic region of the modes, upwind of the cylinder, resemble acoustic multipoles (a dipole in Fig. 3a, a monopole in Fig. 3b and higher-order multipoles in Fig. 3c and Fig. 3d). The modes indicate a clear relation between the vortexes at the wake and the sound waves emitted from the cylinder. The structures associated with the vortexes have wavelengths similar to the structures associated with the noise. This is expected, as the emission of noise and the separation of the flow are caused by the shock waves that appear at the top and bottom of the cylinder.

Figure 4 shows the DMD eigenvalues plotted on the complex plane, along with the unit circle. It is possible to observe that all eigenvalues lie on the unit circle, which means that all the calculated DMD modes are marginally stable, i. e., the amplitudes of the modes remain constant. This is consistent with the original set of flow snapshots, captured when the flow was fully established and periodic.

Reconstruction of The Flow

Figure 5 shows the pressure signals at four different points on the domain, indicated as blue dots in Fig.1b. Figure 5a corresponds to the dot upwind of the cylinder and Fig. 5b, to the dot upwind and above the cylinder. It is possible to observe that, at these positions, the pressure fluctuations are discontinuities, i. e., shock waves that propagate upwind from

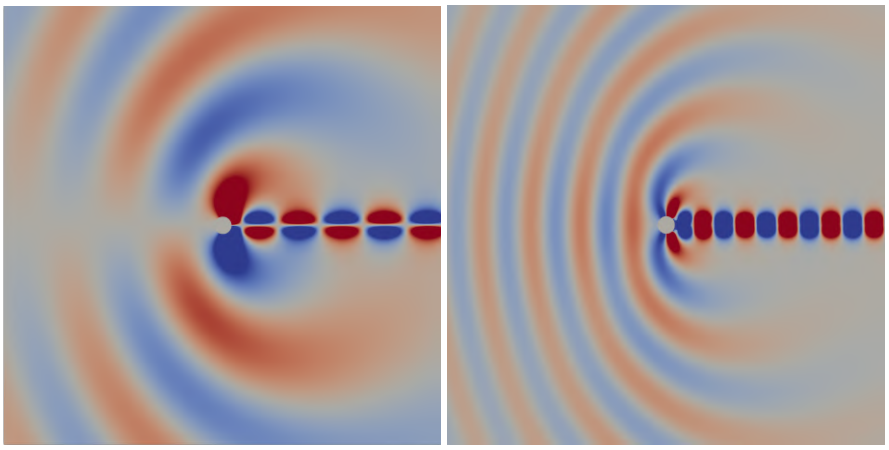

(a) (b)

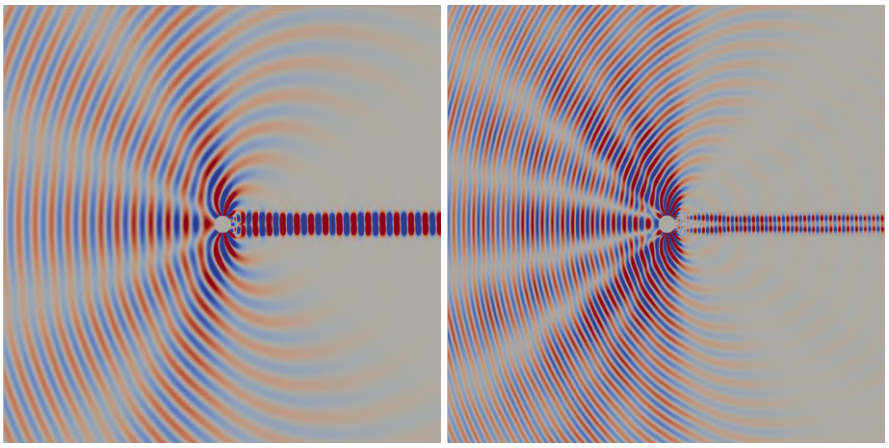

(c) (d)

Figure 3: Selected DMD modes

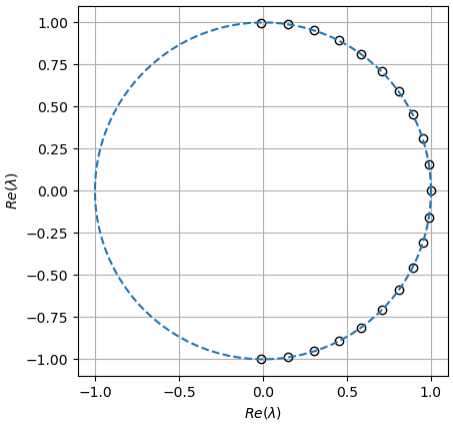

Figure 4: DMD eigenvalues λ.

the cylinder. Figure 5c corresponds to a position downwind of the cylinder, inside the wake. The pressure fluctuations in this position are caused by the passage of the low-pressure vortex cores, and Fig. 5d corresponds to a position downwind of the cylinder but above the wake.

The curves with dashed red lines in Fig. 5 are the reconstruction of the pressure signals using the DMD modes, as shown in Eq. (5). This reconstruction was able to properly capture the peaks of the shock waves upwind of the cylinder, but the expansion just after the shocks is very poorly captured, with pressure fluctuations that do not appear in the original signal. In addition to that, the reconstruction of the signal inside the cylinder wake shows a significant error

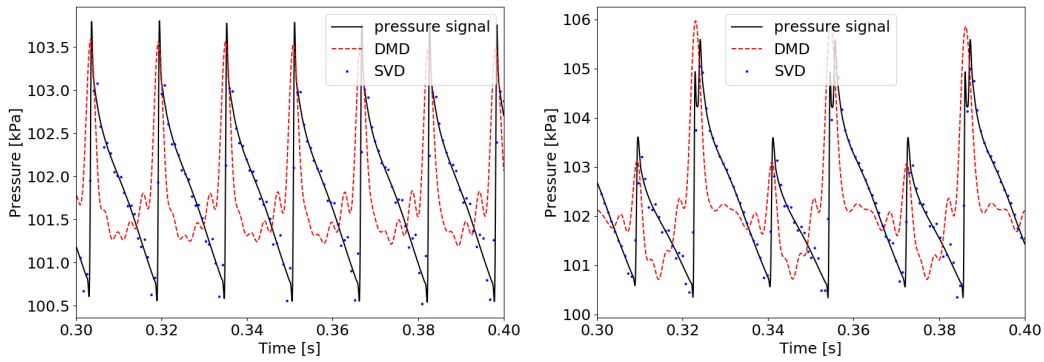

(a) $x = -10, y = 0$ (upwind of cylinder).

(b) $x = -5, y = 2$ (upwind, above cylinder).

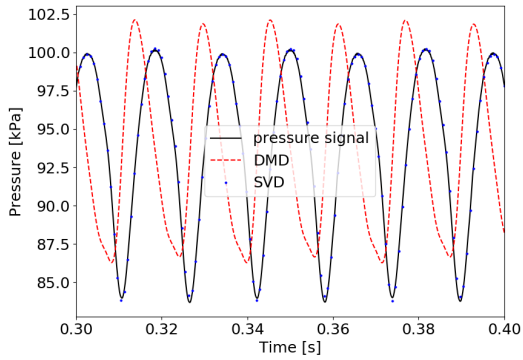

(c) $x = 1, y = 0$ (downwind cylinder).

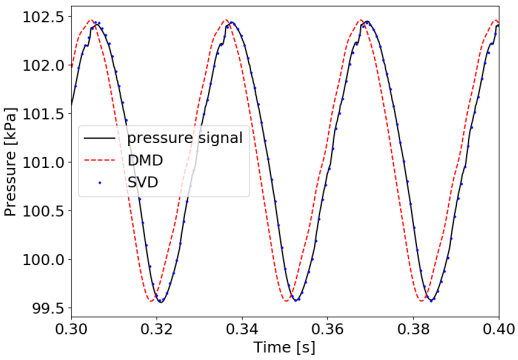

(d) $x = 5, y = 2$ (downwind, above cylinder).

Figure 5: Pressure signal (black continuous), DMD reconstruction with Eq. (5) (red dashed) and left singular vectors reconstruction with Eq. (6) (blue points).

at the mean value of the pressure fluctuations, as well as a large phase shift. This is probably because this position is very close to the cylinder, as can be seen in Fig. 1b. The best result for the reconstruction was for the signal evaluated at a position downwind of the cylinder and outside the wake which has only a small phase shift with respect to the original signal, possibly because the pressure fluctuations in this position are smaller and do not contain large discontinuities or perturbations, as can be seen inf Fig. 1b.

The curves with blue points in Fig. 5 are the reconstruction of the pressure signals using a projection of the snapshots on the columns of the left singular matrix $\mathbf{U}$ from the SVD, whose columns are the left singular vectors, with Eq. (6). It is possible to see from the figures that this reconstruction with the left singular vectors has a much better agreement with the original signal, when compared with the DMD modes. However, this method has the disadvantage of only reconstructing the pressure field at time instants that are multiples of the sampling interval used to generate the snapshots, because, unlike the equation that uses the DMD modes, Eq. (6) does not include the time explicitly.

Figure 6 shows the instantaneous, relative error between one of the original flow snapshots, and the reconstructed flow at the same time instant, defined for each point of the domain as

$$E = 100 \times \frac{|p - p_{dmd}|}{p},$$

were E is the relative error, p is the original pressure value at the same point and p_{dmd} is the pressure value at the point calculated with the DMD modes. It is possible to see that the DMD reconstruction is capable of capturing the shock waves well, with an error close to 1%. However, around the shock waves, the error increases rapidly to around 20% because, as was shown in Figs. 5a and 5b, the expansion after the shock waves is not well captured by the synthesis with DMD modes. At the wake, it is possible to see that the error increases, probably due to the phase difference, and gets to around 100% at certain points. The largest error observed, of over 1,000%, is at the region close to the cylinder wall, just before the shock wave, which is where the flow reaches the maximum velocity. It is also possible to observe that the error is relatively small at the region downwind from the cylinder and far from the flow wake. This is expected, because in this region, the flow is far less complex, when compared to the rest.

Even though Fig. 6 shows many interesting aspects of the difference between the original and the reconstructed flows, the phase shift observed in the reconstructed results shown in Fig. 5c and Fig. 5d, has an important contribution to the error seen in Fig. 6, but is far less relevant to an analysis of the intensity of the generated noise, and can be compensated

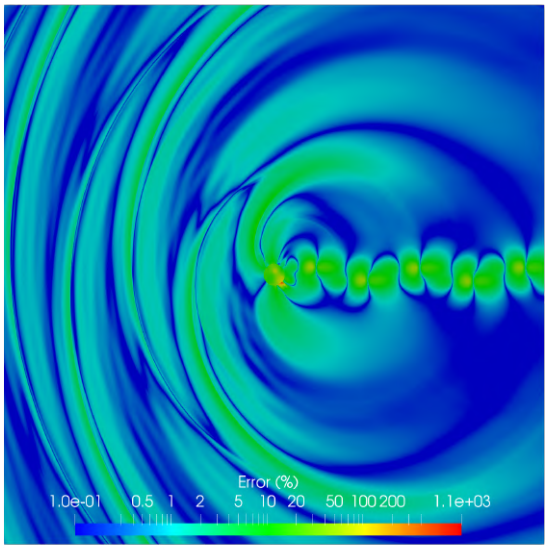

Figure 6: Relative error for the instantaneous flow reconstructed with the DMD modes.

if there is an interest in using the DMD results to other applications such as control. With that in mind, the DMD modes were used to generate a new set of snapshots for the pressure field, and this set was then used to calculate a reconstructed Sound Pressure Level field, using Eq. 7. The error, in decibels, between this reconstructed SPL field and the original, shown in Fig. 2 was calculated as

$$E_{dB} = |SPL - SPL_{DMD}|,$$

where E_{dB} is the error in each point of the domain, SPL is the original Sound Pressure Level at the same point, and SPL_{DMD} is the Sound Pressure Level calculated with the pressure fields reconstructed with the DMD modes. The resulting error is shown if Fig. 7.

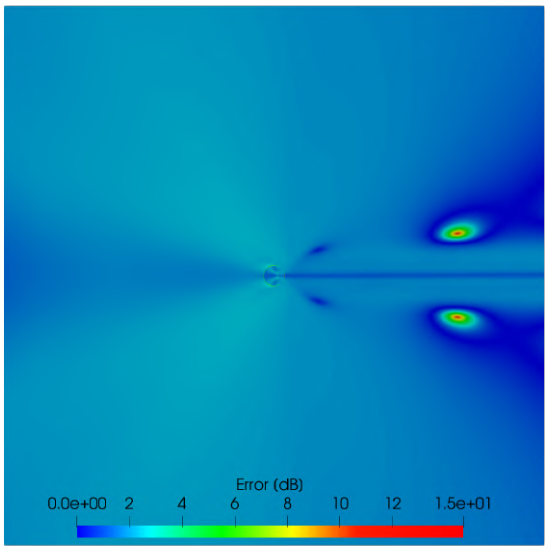

Figure 7: Error for the Sound Pressure Level field reconstructed with the DMD modes.

The error over most of the domain was around 2.5 dB, including the wake region, were the instantaneous error got over 100% at certain points. It is also possible to see that the method was unable to capture the two regions of silence seen above and below the wake in Fig. 2. The DMD reconstruction actually overestimated the Sound Pressure Level in

these regions by about 10 dB. Even though the error for the Sound Pressure Level is relatively small most of the flow field, of about 2 dB when the original SPL is close to 150 dB, it is important to notice that the Sound Pressure Level scale is logarithmic. Therefore, a change of 2 dB actually corresponds to a significant increase in sound intensity. With that in mind, the relative error for the root mean square value of the pressure fluctuations (p'_{rms}) was calculated as

$$E_{rms} = 100 \times \frac{|p'_{rms} - p'_{rmsDMD}|}{p'_{rms}},$$

where E_{rms} is the relative error at a point in the domain, p'_{rms} is the original pressure root mean square value at the same point and p'_{rmsDMD} is the pressure root mean square value calculated with the same set of reconstructed pressure fields used for the SPL error calculation, and the result is shown in Fig. 8.

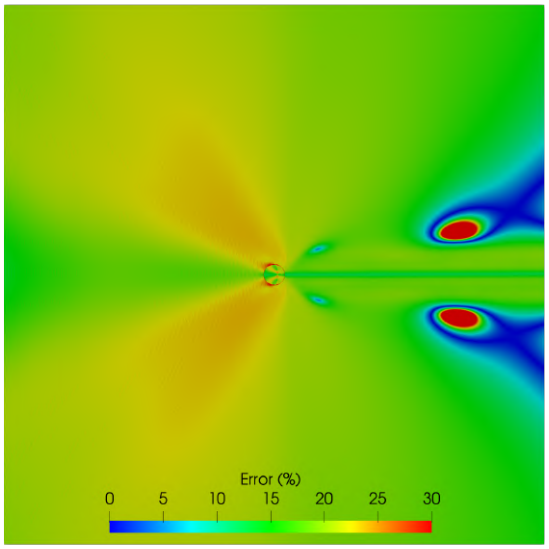

Figure 8: Relative error for the p'_{rms} field reconstructed with the DMD modes.

For most of the flow field, the resulting error varies from approximately 15% to 25%. The error is only higher than 30% near the wall of the cylinder and in the silence regions near the wake, where the maximum error gets above 200%. These values for the error are consistent with the results for the instantaneous error, from Fig. 6, and give a better understanding of the difference between the original flow and the DMD reconstruction, when compared to the SPL error.

CONCLUSIONS

The Dynamic Modes Decomposition was applied to pressure field snapshots for the transonic flow around a cylinder. The structures of the modes associated to the wake are compatible to the structures obtained by Kutz *et al.* (2016), considering the differences between the analyzed data sets. The DMD modes also revealed that the sound generated by the flow can be understood as a combination of several acoustic multipoles with different orders (i. e., a combination of monopoles, dipoles, quadrupoles, etc.). The DMD eigenvalues were all positioned on the unit circle in the complex plane, which indicates that the system is undamped and marginally stable and is consistent with the analyzed flow.

The results for the reconstruction of the pressure signals showed that the use of a projection onto left singular vectors yields more accurate field reconstruction than the use of the DMD modes, but both methods were capable of correctly capturing the frequency and amplitude of oscillation. However, the DMD reconstruction showed inconsistencies with phase and, in some cases, mean values at the wake region of the flow, and was not able to capture the expansions after the shock waves upwind from the cylinder. These results are compatible with those presented by Alenius (2012), who used DMD and POD modes to reconstruct the compressible flow though a thick orifice plate and concluded that the POD was more appropriate than the DMD. The results are also compatible with those from Tissot *et al.* (2014). The authors showed that the classical DMD algorithm, which was used in this paper, had a significantly higher error than an optimised DMD method.

ACKNOWLEDGMENTS

The authors wish to thank the financial support from CAPES and from the Graduate Program in Mechanical Sciences from the University of Brasilia.

REFERENCES

Alenius, E., 2012. *Flow Duct Acoustics - An LES Approach*. Ph.D. thesis, Royal Institute of Technology, Stockholm, Sweden.

Alenius, E., Åbom, M. and Fuchs, L., 2015. "Large eddy simulations of acoustic-flow interaction at an orifice plate". *Journal of Sound and Vibration*, Vol. 345, pp. 162–177. ISSN 0022-460X. doi:https://doi.org/10.1016/j.jsv.2015.02.012. URL https://www.sciencedirect.com/science/article/pii/S0022460X15001467.

Ali, M.Y., Pandey, A. and Gregory, J.W., 2016. "Dynamic mode decomposition of fast pressure sensitive paint data". *Sensors*, Vol. 16, No. 6. ISSN 1424-8220. doi:10.3390/s16060862. URL https://www.mdpi.com/1424-8220/16/6/862.

Belson, B.A., Tu, J.H. and Rowley, C.W., 2014. "Algorithm 945: Modred—a parallelized model reduction library". *ACM Trans. Math. Softw.*, Vol. 40, No. 4. ISSN 0098-3500. doi:10.1145/2616912. URL https://doi.org/10.1145/2616912.

Gowen, F.E. and Perkins, E.W., 1952. "Drag of circular cylinders for a wide range of reynolds numbers and mach numbers". *NACA Research Memorandum*.

Hughes, T.J.R. and Tezduyar, T.E., 1984. "Finite elements method for first-order hyperbolic systems with particular emphasis on the compressible euler equations". *Computer Methods in Applied Mechanics and Engineering*, Vol. 45, pp. 217–284.

Kutz, J.N., Brunton, S.L., Brunton, B.W. and Proctor, J.L., 2016. *Dynamic Modes Decomposition: Data-Driven Modeling of Complex Systems*. Society for Industrial and Applied Mathematics, Philadelphia.

Miserda, R.F.B., Pimenta, B.G. and Da Rocha, L.S., 2020. "Dynamic mode decomposition of numerical and experimental data". *Journal of Fluid Mechanics*, Vol. 36, pp. 363–380.

Nair, V., Alenius, E., Boij, S. and Efraimsson, G., 2016. "Inspecting sound sources in an orifice-jet flow using lagrangian coherent structures". *Computers & Fluids*, Vol. 140, pp. 397–405. ISSN 0045-7930. doi:https://doi.org/10.1016/j.compfluid.2016.09.001. URL https://www.sciencedirect.com/science/article/pii/S0045793016302626.

Nichols, J.W., Larsson, J., Bernardini, M. and Pirozzoli, S., 2017. "Stability and modal analysis of shock/boundary layer interactions". *Theoretical and Computational Fluid Dynamics*, Vol. 31, No. 1, pp. 33–50. doi:10.1007/s00162-016-0397-6. URL https://doi.org/10.1007/s00162-016-0397-6.

Rodriguez, O., 1984. "The circular cylinder in subsonic and transonic flow". *AIAA Journal*, Vol. 22, No. 12, pp. 1713–1718. doi:10.2514/3.8842. URL https://doi.org/10.2514/3.8842.

Sarmast, S., Dadfar, R., Mikkelsen, R.F., Schlatter, P., Ivanell, S., Sørensen, J.N. and Henningson, D.S., 2014. "Mutual inductance instability of the tip vortices behind a wind turbine". *Journal of Fluid Mechanics*, Vol. 755, p. 705–731. doi:10.1017/jfm.2014.326.

Schmid, P.J., 2010. "Dynamic mode decomposition of numerical and experimental data". *Journal of Fluid Mechanics*, Vol. 656, p. 5–28. doi:10.1017/S0022112010001217.

Schmid, P.J., Li, L., Juniper, M.P. and Pust, O., 2011. "Applications of the dynamic mode decomposition". *Theoretical and Computational Fluid Dynamics*, Vol. 25, No. 1, pp. 249–259. doi:10.1007/s00162-010-0203-9. URL https://doi.org/10.1007/s00162-010-0203-9.

Schmid, P.J. and Sesterhenn, J., 2008. "Dynamic mode decomposition of numerical and experimental data". In *61st Annual Meeting of the APS Division of Fluid Dynamics*. American Physical Society.

Tissot, G., Cordier, L., Benard, N. and Noack, B.R., 2014. "Model reduction using dynamic mode decomposition". *Comptes Rendus Mécanique*, Vol. 342, No. 6, pp. 410–416. ISSN 1631-0721. doi:https://doi.org/10.1016/j.crme.2013.12.011. URL https://www.sciencedirect.com/science/article/pii/S163107211400103X. Flow separation control.

Tu, J.H. and Rowley, C.W., 2012. "An improved algorithm for balanced pod through an analytic treatment of impulse response tails". *Journal of Computational Physics*, Vol. 231, No. 16, pp. 5317–5333. ISSN 0021-9991. doi:https://doi.org/10.1016/j.jcp.2012.04.023. URL https://www.sciencedirect.com/science/article/pii/S0021999112002045.

Williams, M.O., Schmid, P.J. and Kutz, N.J., 2013. "Hybrid reduced-order integration with proper orthogonal decomposition and dynamic mode decomposition". *Multiscale Modeling & Simulation*, Vol. 11, No. 2, pp. 522–544. doi: 10.1137/120874539. URL https://doi.org/10.1137/120874539.

RESPONSIBILITY NOTICE

The authors are the only ones responsible for the printed material included in this paper.